Short title: Carboxysome mispositioning alters cell physiology

Article Title: Cyanobacterial growth and morphology are influenced by carboxysome positioning and temperature

Authors: Rees Rillema[1], Joshua S. MacCready[1], Anthony G. Vecchiarelli[1]*

Affiliations: 1. Department of Molecular, Cellular, and Developmental Biology, University of Michigan, Ann Arbor, MI, USA.

***Corresponding Author Email Address**: ave@umich.edu

One Sentence Summary: Carboxysome positioning by the McdAB system influences cyanobacterial growth and cell morphology at environmentally relevant growth temperatures

Author Contributions: All authors conceived the original research plans and project; A.G.V. and J.S.M supervised the experiments; R.R. performed all experiments; J.S.M. provided technical assistance to R.R.; All authors designed experiments and analyzed the data; A.G.V. wrote the article with contributions from R.R. and J.S.M.; A.G.V. agrees to serve as the author responsible for contact and ensures communication.

Funding Information: This work was supported by the National Science Foundation to A.G.V. (Award No. 1817478 and CAREER Award No. 1941966), research initiation funds provided by the MCDB Department to A.G.V., and by research funds from the Michigan Life Sciences Fellows Program to J.S.M.

ABSTRACT

Cyanobacteria are the prokaryotic group of phytoplankton responsible for a significant fraction of global CO_2 fixation. Like plants, cyanobacteria use the enzyme Ribulose 1,5-bisphosphate Carboxylase/Oxidase (RuBisCO) to fix CO_2 into organic carbon molecules via the Calvin-Benson-Bassham cycle. Unlike plants, cyanobacteria evolved a carbon concentrating organelle called the carboxysome - a proteinaceous compartment that encapsulates and concentrates RuBisCO along with its CO_2 substrate. In the rod-shaped cyanobacterium *Synechococcus elongatus* PCC7942, we recently identified the McdAB system responsible for uniformly distributing carboxysomes along the cell length. To date, it is unclear what role carboxysome positioning plays with respect to cellular physiology. Here, we show that a failure to distribute carboxysomes leads to a temperature-dependent decrease in cell growth rate, changes in cell morphology, and a significant reduction in cellular levels of RuBisCO. Unexpectedly, we also found that wild-type *S. elongatus* elongates and divides asymmetrically at the environmentally relevant growth temperature of 20°C. We propose that carboxysome positioning by the McdAB system functions to maintain carbon-fixation efficiency of RuBisCO by preventing carboxysome aggregation, which is particularly important at temperatures where rod-shaped cyanobacteria adopt a filamentous morphology.

INTRODUCTION

Cyanobacteria represent a phylum of diverse prokaryotic organisms where many fundamental biological processes have remained largely understudied. As the evolutionary ancestor of algae and plant chloroplasts, all cyanobacteria perform oxygenic photosynthesis and fix carbon dioxide through the Calvin-Benson-Bassham cycle. Unlike chloroplasts, cyanobacteria encapsulate their RuBisCO and carbonic anhydrase within large (~150 nm) selectively permeable protein-based organelles called carboxysomes. This mechanism generates an environment around RuBisCO that is significantly enriched in CO_2, which increases the carboxylation activity of RuBisCO, while simultaneously reducing photorespiration (Rae et al., 2013).

In the model rod-shaped cyanobacterium *Synechococcus elongatus* PCC 7942 (hereafter *S. elongatus*), carboxysomes were found to be uniformly distributed down the length of individual cells (Savage et al., 2010). This equidistant positioning supports equal inheritance of carboxysomes following cell division and maximum diffusion of substrates and products across the carboxysome shell. Carboxysomes are essential for the growth and survival of all cyanobacteria and is responsible for ~35% of global carbon-fixation through atmospheric CO_2 assimilation (Dworkin, 2006; Kerfeld and Melnicki, 2016). Therefore, understanding how the subcellular organization of carboxysomes influences cyanobacterial physiology is of considerable ecological, evolutionary, and biotechnological importance, yet remains unclear.

Savage *et. al.* were first to report that a ParA-type ATPase (hereafter McdA - Maintenance of carboxysome distribution A) is required for positioning carboxysomes in *S. elongatus* (Savage et al., 2010). ParA family members have well established roles in the segregation of bacterial chromosomes and plasmids (Baxter and Funnell, 2014; Badrinarayanan

et al., 2015). Less studied are ParA family members shown to be required in the positioning of diverse protein complexes, such as those involved in secretion (Viollier et al., 2002; Perez-Cheeks et al., 2012), chemotaxis (Thompson et al., 2006; Ringgaard et al., 2011; Alvarado et al., 2017), conjugation (Atmakuri et al., 2007), cell division (Raskin and De Boer, 1999; Jordan et al., 2017), and cell motility (Youderian et al., 2003; Kusumoto et al., 2008), as well as bacterial microcompartments (BMCs), such as the carboxysome (Savage et al., 2010; MacCready et al., 2018). We recently identified a small novel protein, McdB, responsible for generating dynamic McdA gradients on the nucleoid (MacCready et al., 2018). McdB colocalizes and directly interacts with carboxysomes and removes McdA from the nucleoid in their vicinity. We found that carboxysomes use a Brownian-ratchet mechanism whereby McdB-bound carboxysome motion occurs in a directed and persistent manner toward increased concentrations of McdA on the nucleoid. We also recently found that the McdAB system is widespread among β-cyanobacteria (MacCready et al., 2020); an incredibly diverse and widely distributed phylum of bacteria that display complex morphologies (Shih et al., 2013). Together, the data suggest that the equidistant positioning of carbon-fixing carboxysomes is a very important mode of subcellular organization for cyanobacterial physiology.

When Savage *et. al.* first identified the McdA requirement for carboxysome positioning, only a minor decrease in CO_2 fixation was found in a Δ*mcdA* strain, but growth under ambient CO_2 was the only condition studied (Savage et al., 2010). *Synechococcus* species are widely distributed throughout coastal and oceanic environments from the equator to high latitudes (Huang et al., 2012; Flombaum et al., 2013). Therefore, when studying changes in cyanobacterial physiology, it is prudent to investigate potential changes under a wide range of growth conditions. Rising sea surface temperatures and coastal eutrophication in marine ecosystems are

pervasive effects of climate change (Doney et al., 2012). Rising temperatures increase enzyme kinetics (Geider, 1987), leading to higher rates of protein synthesis, RuBisCO activity, and photosynthesis (Raven and Geider, 1988). Temperature therefore directly influences cyanobacterial growth and metabolic rates (Eppley, 1972; Chen et al., 2014). Here we find temperature-dependent changes in *S. elongatus* growth rate and cell morphology that are associated with carboxysome mispositioning in Mcd system mutants.

RESULTS

We performed *in vivo* microscopy to determine how carboxysome organization was altered in the cell populations of *mcdA*, *mcdB*, and *mcdAB* deletion strains compared to wild-type *S. elongatus*. In *S. elongatus*, each RuBisCO enzyme is composed of eight Large (RbcL) and eight Small (RbcS) subunits to form $RbcL_8S_8$ (Tabita et al., 2008). Therefore, to image carboxysomes, the fluorescent protein mTQ (monomeric Turquoise2) was fused to the C-terminus of RbcS to make RbcS-mTQ (see Methods for strain construction details). *RbcS-mTQ* was expressed using a second copy of its native promoter (inserted at neutral site 1) in addition to wild-type *rbcS* at its native locus in wild-type cells as well as in the three deletion strains – Δ*mcdA*, Δ*mcdB*, and Δ*mcdAB*. Carboxysomes of *S. elongatus* encapsulate between 800 to 1,500 RuBisCO enzymes (Sun et al., 2019). Therefore, RbcS-mTQ provides a bright and high-contrast marker for quantifying the subcellular organization of carboxysomes, as previously shown (MacCready et al., 2018). We also performed Phase Contrast imaging to monitor for potential changes in cell morphology, and Chlorophyll fluorescence imaging to verify that cells were photosynthetically active and therefore viable.

S. elongatus PCC 7942 was originally isolated from a fresh water source in the San Francisco bay area, with an annual temperature range of 8°C to 25°C (Welkie et al., 2019). In the lab however, *S. elongatus* is typically grown at 32°C because of its slow doubling time; on the order of several hours depending on growth conditions (temperature, light, and CO_2 availability). This was the temperature used in our previous study that identified the McdAB carboxysome positioning system (MacCready et al., 2018). *S. elongatus* has recently been shown to grow slightly faster at 40°C (Yu et al., 2015; Ohbayashi et al., 2019). In anticipation of a growth defect in the absence of carboxysome positioning in our Mcd system mutants, we began our studies by growing cultures at 40°C in constant light under ambient (0.04%) or high (2%) CO_2 concentrations.

Carboxysome mispositioning correlates with minor defects in cellular physiology at 40°C

We first verified that carboxysomes are organized by the McdAB system at 40°C, as we found previously at 32°C (MacCready et al., 2018). We examined carboxysome positioning under high CO_2 conditions (2% CO_2) to maximize growth. We found that RbcS-mTQ labeled carboxysomes were equally spaced down the long axis of wild-type *S. elongatus* cells **(Figure 1A)**. The Δ*mcdA*, Δ*mcdB*, and Δ*mcdAB* mutants lost this uniform positioning of carboxysomes **(Figure 1B-D)**; as observed previously at 32°C (MacCready et al., 2018).

We compared the nearest-neighbor spacing of carboxysome foci as a function of cell length **(Figure 1E)**. Wild-type cells showed uniform carboxysome spacing (0.55 ± 0.20 μm) regardless of cell length. All three mutants, on the other hand, displayed a gradual increase in the nearest-neighbor spacing of carboxysome foci as cell length increased. Both the average and variability in spacing were greater in the mutants compared to wild-type **(Figure 1F)**. The

increased spacing resulted in fewer carboxysome foci per cell **(Figure 1G)**, and within single cells, there were fewer carboxysome foci per unit cell length **(Figure 1H)**. When comparing the fluorescence intensity **(Figure 1I)** and diameter of carboxysome foci **(Figure 1J)**, it became apparent that the increased spacing in all three mutant populations was not likely a result of fewer carboxysomes being assembled, but rather, the result of carboxysomes coalescing into massive aggregates. Indeed, when comparing carboxysome foci number across cell populations, we find that ~ 95 % of wild-type cells (n = 440) had 3 or more foci, whereas ~ 80 % of all three mutant populations had 3 or fewer foci **(Figure 1K)**. Roughly 20% of cells from all three mutant populations had a single carboxysome aggregate. Consistent with what we have shown previously (MacCready et al., 2018), the 40°C data shows that the McdAB system not only equally spaces carboxysomes down the cell length, it also serves as an anti-aggregator; preventing carboxysomes from coalescing.

We asked if carboxysome mispositioning affected cell growth at 40°C. Wild-type *S. elongatus* cells were 3.1 ± 0.5 microns in length **(Figure 2A)** and 1.25 ± 0.05 microns in width **(Figure 2B)**. We found that Δ*mcdA* cells were of a similar length and width compared to that of wild-type **(Figure 2AB)**. The Δ*mcdB* and Δ*mcdAB* mutant populations had a slightly longer average cell length, but a significantly greater distribution in length **(Figure 2A)**. The presence of both longer and shorter cells suggests that a small fraction (~ 5%) of the Δ*mcdB* and Δ*mcdAB* populations were undergoing asymmetric cell division. These mutants were also slighter thinner in width compared to wild type cells **(Figure 2B)**. The data suggest that while both McdA and McdB are required for positioning carboxysomes, the loss of McdB elicits a subtle asymmetric division phenotype across a minor fraction of the cell population at 40°C.

The changes in cell morphology suggested that, even with high CO_2 levels, carboxysome mispositioning may alter cell growth. However, we only found a very modest reduction in growth rate for all three mutants **(Figure 2C-D)**. Even when grown slowly in ambient CO_2 (0.04%), we did not observe significant differences in growth rate compared to wild-type **(Figure 2E-F)**. Overall, at 40°C, we find that carboxysomes are mispositioned in all three Mcd mutants, with moderate increases in carboxysome spacing due to aggregation, which ultimately resulted in fewer carboxysome foci per cell. Modest changes in cell morphology were detected only in strains where McdB was absent. In all three deletion strains, growth rate was not significantly slower, with or without CO_2, at this temperature.

Carboxysome mispositioning correlates with cell division arrest, cell elongation, and asymmetric cell division at 30°C

We continued our study at 30°C, a growth temperature closer to what we used to first identify the McdAB carboxysome positioning system (MacCready et al., 2018). As we showed previously, and similar to our 40°C data, wild-type *S. elongatus* cells have equally spaced carboxysomes **(Figure 3A)**, while in all three mutants, carboxysomes were irregularly-spaced **(Figure 3B-D)**. When we compared the nearest-neighbor spacing of carboxysome foci as a function of cell length, wild-type showed the same uniform spacing (0.50 ± 0.20 mm) regardless of cell length **(Figure 3E)**, as shown at 40°C **(see Figure 1E)**. All three mutants, on the other hand, displayed increased spacing, and variability in spacing, as cell length increased **(Figure 3E)**. Intriguingly, it also became apparent that mutant cell lengths were significantly longer compared to wild-type. This cell elongation phenotype was more extreme in the Δ*mcdB* and Δ*mcdAB* mutants, resulting in more distantly spaced carboxysome foci **(Figure 3F)**. The data

once again suggests that McdB plays a currently unknown role in carboxysome function, separate from its role in positioning with McdA.

The increased spacing resulted in fewer carboxysome foci per cell **(Figure 3G)**, and within single cells, there were fewer carboxysome foci per unit cell length **(Figure 3H)**. Carboxysome foci in all three mutants were significantly larger than that of wild-type, suggesting aggregation **(Figure 3I-J)**. While ~ 90 % of wild-type cells (n = 486) had 3 or more foci, ~ 70 % of all three mutant populations had 3 or fewer foci **(Figure 3K)**. Again, ~ 20 % of cells in all three mutant populations contained a single carboxysome aggregate. This is a striking reduction in carboxysome foci when considering the cell elongation phenotype exclusive to the mutant cell lines.

As the carboxysome spacing data suggested, mutants were significantly longer than wild-type cells when grown at 30°C **(Figure 4A)**. The presence of elongated cells, as well as cells of wild-type length, suggests that cell division is being inhibited, and when division does occur, it is asymmetric. The Δ*mcdA* cells were of a similar width to that of wild-type, while Δ*mcdB* and Δ*mcdAB* cell populations displayed significantly wider distributions in cell width **(Figure 4B)**. We propose that carboxysome mispositioning and aggregation at 30°C elicits cell division arrest, cell elongation and asymmetric cell division; phenotypes that were largely masked when cells were grown at 40°C.

The changes in cell morphology suggested that the mutants may display slower growth rates, even when grown at high CO_2. However, once again, that was not the case. Under high CO_2 conditions, no significant reduction in growth rate was observed for all three mutants when compared to wild-type **(Figure 4C-D)**. Even when grown in ambient CO_2, reductions in growth rate of the mutants were minor **(Figure 4E-F)**. Overall, we find that at 30°C, carboxysomes are

mispositioned in the Δ*mcdA*, Δ*mcdB*, and Δ*mcdAB* mutants; with drastic increases in carboxysome spacing due to aggregation, which resulted in fewer carboxysome foci per cell. Strikingly, we unveiled cell-division inhibition and asymmetric cell division phenotypes for all three mutant populations at 30°C, which were largely masked at 40°C **(compare Panel A in Figures 2 and 4)**. Despite the carboxysome aggregation and cell-division phenotypes, only minor decreases in growth rate were observed, even with atmospheric levels of CO_2. We propose that at 30°C, carboxysome aggregation decreases the carbon-fixing activity of encapsulated RuBisCO, which triggers a carbon-limitation response - cell division arrest and elongation

S. elongatus elongates at 20°C and this mode of growth is slower in Mcd system mutants

A ten degree drop in temperature unveiled a physiological phenotype at 30°C that was masked at 40°C. We therefore decided to study the effects of carboxysome mispositioning when cells were grown at 20°C, which is within the environmentally relevant temperature range of this isolate of *S. elongatus* (Flombaum et al., 2013). Unexpectedly, we found that even wild-type *S. elongatus* undergoes dramatic cell elongation when grown at 20°C **(Figure 5A)**. *S. elongatus* has been previously studied at this temperature (Burns et al., 2005), but to our knowledge, this is the first time cell morphology has been directly observed. Despite the dramatically long cell lengths, carboxysomes were still robustly aligned down the entirety of the cell length **(Figure 5A)**. All three mutants were also elongated, but to a lesser extent, and carboxysomes were clearly mispositioned **(Figure 5B-D)**.

When we compared the nearest-neighbor spacing of carboxysome foci as a function of cell length, wild-type showed the same uniform spacing (0.50 ± 0.30 μm) even in cells that were almost 20 microns long **(Figure 5E)**. All three mutants, on the other hand, displayed

dramatically increased nearest-neighbor spacing, and variability in spacing, as cell length increased **(Figure 5F)**. Consistently, all three mutants had significantly fewer carboxysome foci per cell **(Figure 5G)**, and within single cells, there were fewer carboxysome foci per unit cell length **(Figure 5H)**. Carboxysome foci in all three mutants were significantly larger than that of wild-type, suggesting carboxysome aggregation **(Figure 5I-J)**. Interestingly, the RbcS-mTQ intensity in carboxysome foci increased in all cell types with decreasing growth temperature **(Supplemental Figure S1)**. This finding is consistent with previous studies showing that RuBisCO abundance in phytoplankton populations inversely correlates with growth temperature (Young et al., 2015). While ~ 90% of wild-type cells (n=388) had 6 or more foci, ~ 90% all three mutant populations had 6 or fewer foci **(Figure 5K)**. Since all cell types elongated at 20°C, the loss of carboxysome positioning in the mutant cell lines represents a massive reduction in carboxysome foci. The data implicates carboxysome positioning by the McdAB system as a requirement for maximizing carbon-fixation in cells that are elongated when grown at cooler but environmentally relevant temperatures.

We quantified cell elongation at 20°C and found that wild-type cells were significantly longer than all three mutants **(Figure 6A)**. The Δ*mcdA* cells were similar in width to that of wild-type, while Δ*mcdB* and Δ*mcdAB* cell populations were notably thinner **(Figure 6B)**. When growth rates were assayed with high CO_2 **(Figure 6C-D)** or ambient CO_2 **(Figure 6E-F)**, we found statistically significant reductions in growth rate for all three mutants when compared to wild-type.

Overall, we identified a cell elongation phenotype in wild-type *S. elongatus* cells that occurs when grown at colder, but environmentally relevant temperatures. All three Mcd mutants elongated to a lesser extent and have aggregated carboxysomes, which resulted in drastically

fewer carboxysome foci per cell compared to wild-type. Significant decreases in growth rate were observed, even with high CO_2 present. The findings suggest that in mutant and wild-type cells, colder growth temperatures decrease the enzyme kinetics of RuBisCO to the point where cell division arrest is triggered in response to carbon-limitation. At 30°C, this response was only found in the Mcd mutants likely due to defects in carbon-fixation efficiency that result from carboxysome aggregation. At 40°C, the enzyme kinetics of RuBisCO are fast enough to compensate for carboxysome aggregation, which would explain why Mcd mutants largely display wild-type cell morphology at high growth temperatures.

Mcd mutants have significantly decreased levels of intracellular RuBisCO

RuBisCO is the sole enzyme providing organic carbon to cellular biomass production and phototrophic growth of *S. elongatus*. Therefore, we set out to determine if carboxysome mispositioning and changes in cell morphology of Mcd mutants at 30°C correlated with altered cellular levels of RuBisCO. Immunoblot analysis against the Large subunit of RuBisCO (RbcL) showed that RuBisCO content is roughly half in all three mutants compared to wild-type cells **(Figure 7A-B)**. RbcL content from cell cultures was normalized based on AtpB quantity from immunoblot analysis as shown previously (Zhang et al., 2012; Sun et al., 2016). The data suggest that although the mutants house massive carboxysome aggregates that are much brighter than those uniformly positioned in wild-type cells **(Supplemental Figure S1)**, the loss of a functioning McdAB system results in a reduction in total cellular RuBisCO content. We speculate that carboxysome mispositioning and aggregation results in a lower level of cellular RuBisCO due to losses in carboxysome integrity and leakage, enzyme stability, and/or degradation. Perhaps related to this hypothesis, it was recently found in *Synechococcus* sp. PCC

7002 that mispositioning of inactivated carboxysomes towards the cell-poles is strongly correlated with their rapid degradation (Hill et al., 2020).

DISCUSSION

We recently identified the McdAB system responsible for the equidistant positioning of carboxysomes down the length of the rod-shaped cyanobacterium *S. elongatus* PCC 7942 (MacCready et al., 2018). We also recently found that McdAB systems are widespread among β-cyanobacteria (MacCready et al., 2020). These findings suggest important and widespread, but currently unknown, physiological roles for carboxysome positioning in these photoautotrophs. Here we find temperature-dependent changes in cell physiology that correlate with carboxysome mispositioning in *mcdA*, *mcdB*, and *mcdAB* deletion strains of *S. elongatus.*

At the three temperatures tested (20, 30, and 40°C), all three mutant cell-types housed few and irregularly spaced carboxysome aggregates, compared to wild-type cells with uniformly-spaced and -sized carboxysome foci. The data supports previous findings that the McdAB system equally distributes carboxysomes to opposite sides of the cell to ensure their inheritance following cell division (Savage et al., 2010; MacCready et al., 2018), akin to ParA-based plasmid partition systems in bacteria (Baxter and Funnell, 2014). But in addition, and particularly important for protein-based cargoes, the McdAB system serves to prevent carboxysome aggregation. This ‘anti-aggregation’ activity serves as a homeostasis mechanism, regulating carboxysome size as well as copy number in the cell. It has recently been found that the pyrenoid, a functionally-analogous organelle to the carboxysome found in the chloroplasts of the model alga *Chlamydomonas*, is also spatially regulated and this activity affects carbon-

fixation (Itakura et al., 2019). It remains to be seen if other BMCs also use spatial regulation mechanisms to avoid aggregation during their self-assembly to optimize enzymatic efficiency.

Physiological defects associated with carboxysome mispositioning are temperature-dependent.

Despite the drastic mispositioning and aggregation of carboxysomes in the *mcdA*, *mcdB*, and *mcdAB* deletion strains of *S. elongatus*, only minor changes in cell morphology and growth rate were detected compared to wild-type at the most optimal growth temperature used in this study (40°C) **(Figures 1 and 2)**. At 30°C however, all mutants displayed cell division arrest, filamentous growth, and asymmetric cell division **(Figure 4)**. Despite significant increases in cell length, the growth rates were not significantly different to that of wild-type; even in ambient CO_2. At our coldest, but environmentally relevant growth temperature of 20°C, we found that even wild-type *S. elongatus* cells undergo filamentous growth. Wild-type cells at 20°C were 5 to 10-times longer than the average length when grown at 30°C or 40°C. Even in these extremely elongated cells, the McdAB system robustly distributed carboxysomes down the entire cell length **(Figure 5A)**. This mode of filamentous growth was slower in all Mcd system mutants, resulting in significantly shorter filaments compared to wild-type **(Figure 6)**. Overall, we find temperature-dependent physiological defects associated with carboxysome mispositioning and aggregation, which were masked at high growth rates and temperatures, and unveiled at lower, but environmentally relevant temperatures.

Cyanobacteria are known to change morphology to increase survival in a myriad changing environmental conditions (Singh and Montgomery, 2011). But currently, the only other known example of cold-induced changes to cyanobacterial morphology is the formation of

akinetes – enlarged and terminally differentiated spore-like cells that allow survival under unfavorable growth conditions (Flores and Herrero, 2010; Kaplan-Levy et al., 2010). Intriguingly, akinete formation is also triggered by carbon-limitation.

Cyanobacteria and chloroplasts have both evolutionary and functional relationships. Chloroplasts are highly sensitive to low-temperature growth, or "chilling stress", which inhibits photosynthesis and carbon fixation (Lee et al., 2007). Typically, the first manifestation of chilling is the swelling and disorganization of chloroplasts - reduced size and number of starch granules, and a distortion and swelling of thylakoids (Kratsch and Wise, 2000).

Cell division arrest and filamentation – A stress response to carbon-limitation?

Our findings suggest that cell division arrest and filamentation are responses triggered by carbon-limitation, resulting from reduced carbon-fixation activity by RuBisCO in carboxysomes. A carbon-limitation response parsimoniously explains the two triggers identified here: (1) carboxysome aggregation and (2) colder growth temperatures. Wild-type cells have carboxysomes of a homogenous size, and as cells grow, so do the number of carboxysomes and their net surface area. The net surface area of the carboxysome shell, where RuBisCO substrates and products interface with the cytoplasm, significantly decreases in our Mcd system mutants due to carboxysome aggregation. As a result, substrate and product permeability is no longer optimal, which could lead to decreased carbon-fixation rates by encapsulated RuBisCO. We propose that cell filamentation is a carbon-stress response used by *S. elongatus* to compensate for decreases in the effective surface area of aggregated carboxysomes. Cell filamentation (i) prevents the birth of cells devoid of carboxysomes, (ii) gives the cell an opportunity to increase carbon-fixation by producing more RuBisCO as a larger aggregate, or by nucleating the

formation of additional carboxysomes *de novo* elsewhere along the elongated cell and (iii) the increased cell-surface area would increase the light-harvesting capability for photochemistry.

We propose this adaptive response to carbon-limitation is also triggered by low temperature growth even in wild-type *S. elongatus*. At high temperature (i.e. 40°C), RuBisCO activity is high (Galmés et al., 2016) and sufficient to compensate for carboxysome mispositioning and RuBisCO aggregation in Mcd system mutants. Therefore, the carbon-limitation response is not triggered. At 30°C, RuBisCO activity is still high enough to prevent a carbon-limitation response in wild-type cells, but not in Mcd mutants with few and aggregated carboxysomes. As a result, cell filamentation is triggered only in the Mcd mutants. At 20°C, RuBisCO activity has reduced to a level that, even in wild-type cells, triggers the carbon-limitation response. Mcd mutants are starved for carbon to the point where growth is slowed, resulting in shorter filaments compared to wild-type.

Spatial regulation of carboxysomes influences RuBisCO activity and abundance

The catalytic rate of RuBisCO is often considered the bottle neck of photosynthesis because the enzyme is inefficient (Erb and Zarzycki, 2018) and temperature dependent (Geider, 1987). The light reactions of photosynthesis, however, are considered temperature independent (Geider, 1987; Ensminger et al., 2006). Psychrophilic phytoplankton species deal with low temperatures, well below the thermal optimum of most enzymes, by increasing the abundance of RuBisCO (Young et al., 2015). It has recently been found that low temperature growth (18 to 22°C) results in increased RuBisCO levels in the marine cyanobacterium *Synechococcus* PCC 7002, compared to growth at 26°C or 30°C (Fernández-González et al., 2020). This trend was also observed in natural phytoplankton assemblages across a wide latitudinal range. Consistently,

we find here that the RbcS-mTQ signal within carboxysome foci across all cell types inversely correlated with decreasing growth temperatures **(Supplemental Figure S1)**.

Previous studies have also shown positive relationships between growth rate and RuBisCO abundance (Falkowski et al., 1989; Raven and Johnston, 1991; Losh et al., 2012; Losh et al., 2013; Young et al., 2015; Fernández-González et al., 2020). Elevated carbon fixation rates during blooms in polar regions have been shown to be associated with several-fold increases in RuBisCO. 20°C is well below the thermal optimum for RuBisCO activity (Galmés et al., 2013), and well below the optimal growth temperature of *S. elongatus*. We therefore conclude that increasing RuBisCO abundance and triggering cell elongation both represent acclimation responses that compensate for the decreased catalytic rate of RuBisCO at low-temperature growth. This response is further compounded when carboxysomes are mispositioned and aggregated in our Mcd mutants. It is important to note that filamentation occurred here under high CO_2 – a condition whereby *S. elongatus* does not require the carbon-concentrating activity of carboxysomes for growth (Cameron et al., 2013). Therefore, the evidence further supports that it is not CO_2 substrate limitation causing filamentation, but rather RuBisCO activity that is significantly compromised when complexed in carboxysome aggregates or when cells are grown at colder temperatures. These findings shed light on the importance of the McdAB system in maximizing the carbon-fixation activity of RuBisCO by preventing carboxysome aggregation during self-assembly.

Overall, we show that carboxysomes are organized by the McdAB system in cyanobacteria and can appropriately respond to variability in RuBisCO abundance and activity along a wide temperature gradient. Our results suggest that carboxysome homeostasis provided by the McdAB system is part of an autotrophic growth strategy in elongated cells - RuBisCO

abundance increases and is distributed into homogeneously-sized carboxysomes at low temperature to overcome the lower catalytic rates of this temperature-dependent enzyme (Young et al., 2015).

McdB plays a role in carboxysome function outside of its positioning with McdA

Regardless of growth temperature, Δ*mcdB* and Δ*mcdAB* mutants elicited stronger cell elongation and asymmetric division phenotypes compared to Δ*mcdA*. Our findings suggest that McdB plays a currently unknown role in carboxysome function, outside of its role in positioning with McdA. Consistently, our recent bioinformatics analysis of McdAB systems across cyanobacteria identified numerous species with orphan McdBs, suggesting functional roles independent of McdA (MacCready et al., 2020). We have also shown previously via bacterial two-hybrid analysis that McdA does not physically associate with any carboxysome component, while McdB directly interacts with a number of shell proteins (MacCready et al., 2018). We have also recently found that purified McdB undergoes Liquid-Liquid Phase-Separation (LLPS) *in vitro* (MacCready et al., 2020). This activity is intriguing given recent studies showing that both α- and β-carboxysomes as well as the algal pyrenoid have components with LLPS behaviors (Freeman Rosenzweig et al., 2017; Wang et al., 2019; Oltrogge et al., 2020). Collectively, these studies suggest that LLPS is a common feature underlying carboxysome biogenesis. It is intriguing to speculate that the LLPS activity of McdB and the carboxysome are related and potentially influence each other.

Cold growth temperature induces elongation and asymmetric cell division

Across the bacterial world, complex systems maintain cell-size homeostasis. We find here that *S. elongatus* maintains cell-size homeostasis when grown at 30°C or 40°C, but undergoes filamentation when grown at the environmentally-relevant temperature of 20°C. A growing number of bacterial species are known to elongate into a filamentous morphology amidst environmental changes to promote survival. For example, *E. coli* cells become filamentous during infection (Justice et al., 2004; Horvath et al., 2011), and during DNA damage, the SOS response blocks cell division until damage has been repaired, resulting in elongation (Kreuzer, 2013). Several other forms of stress have been shown to induce elongation, including host environment, antibiotics, nutrient access, pH, heat shock, and osmotic fluctuations (Justice et al., 2008; Bos et al., 2015; Wehrens et al., 2018; Heinrich et al., 2019). Bacteria can clearly exist in diverse morphological states, in part dictated by their environment (Kysela et al., 2016; Yang et al., 2016).

To our knowledge, we find here the first example of bacterial filamentation caused by cold-growth temperature. We propose colder temperatures trigger filamentation indirectly as a carbon-limitation response due to the reduced carbon-fixing activity of RuBisCO. Alternatively, transition into a filamentous morphology has been proposed to confer advantages, such as avoiding phagocytosis via the host immune response (Justice et al., 2004; Justice et al., 2008; Horvath et al., 2011; Yang et al., 2016) or to protect against predation in aquatic environments (Wortinger et al., 1998; Pernthaler et al., 2004; Pernthaler, 2005; Heinrich et al., 2019). It is attractive to speculate that the growth temperature of 20°C coincides with the seasonal temperature during which predation occurs (Pernthaler et al., 2004). That is, *S. elongatus* may use temperature as a cue to elongate so as to avoid planktivorous protists. Consistent with this possibility, previous studies have demonstrated that several freshwater bacteria, including

Caulobacter crescentus (Heinrich et al., 2019), exhibit high phenotypic plasticity and can transition to a filamentous morphology – a transition that may be specifically triggered in the presence of a size-selective protistan predator (Simek et al., 1997; Hahn et al., 1999; Pernthaler et al., 2004). It is possible that some aquatic bacteria have evolved to undergo filamentation at temperatures that coincide with grazing season.

Several studies have characterized the mechanisms by which bacterial filamentation is induced, particularly under DNA damage or exposure to antibiotics (Kreuzer, 2013). But how bacterial cells enter and exit these filamentous states to ensure survival during changes in environment remains poorly characterized and is a recent question of interest. We find here that *S. elongatus* forms filaments when grown at low temperature or when carboxysomes are mispositioned. When these filaments divide, it is asymmetric – forming a daughter cell of 'normal' length. It has been recently shown that *S. elongatus* can also be induced to filament under dim-light stress, and then divides asymmetrically to form daughter cells of the correct size when brought back into well-lit conditions (Liao and Rust, 2018). Somewhat related, the Chlorophyll signals along the length of our Mcd mutant cell-lines was much more heterogeneous, particularly at 20°C, compared to wild-type **(see Figure 5A-D)**. It should be noted that in addition to sensing light and inorganic carbon substrates, *S. elongatus* responds to lowering temperatures by slowing and even turning off circadian rhythms; thereby down regulating cell growth, division, and metabolic flux (Murayama et al., 2017; Broddrick et al., 2019).

The Min system has been shown to play a role in the asymmetric cell division and daughter-cell sizing of filamentous *E. coli* (Wehrens et al., 2018), *V. parahaemolyticus* (MacCready and Vecchiarelli, 2018; Muraleedharan et al., 2018), and *S. elongatus* (Liao and

Rust, 2018). Recent findings suggest that division restoration at the poles of these filaments is regulated by a combination of Min oscillations, FtsZ levels and *terminus* segregation, resulting in daughter cells of the right length (Cayron et al., 2020; Raghunathan et al., 2020). The mechanism by which filamentation and asymmetric division occurs in *S. elongatus* is an area of future research. Taken together, the conserved ability for various bacterial species to undergo filamentation and morphological recovery, some of which showing direct selective benefits, strongly suggests that this differentiation plays an important role in survival and proliferation.

MATERIALS AND METHODS

Construct designs. All constructs in this study were generated using Gibson Assembly (Gibson et al., 2009) from synthetized dsDNA and verified by sequencing. Constructs contained flanking DNA that ranged from 500 to 1500 bp in length upstream and downstream of the targeted insertion site to promote homologous recombination into target genomic loci (Clerico et al., 2007).

Generation of Bacterial Strains. All *Synechococcus elongatus* PCC7942 transformations were performed as previously described (Clerico et al., 2007). Plasmid constructs of *mcdA*, *mcdB*, and *mcdAB* deletions were created by replacing the respective coding sequences with a kanamycin resistance cassette. All fluorescent strains were transformed using plasmid pAH40, which contains a chloramphenicol resistance cassette and a second copy of the *rbcS* promoter and gene, attached at the 3' end with the gene encoding for fluorescent protein mTurquoise2 (mTQ) and separated with a GSGSGS linker, inserted into neutral site 1. Transformed cells were plated on BG-11 agar. Single colonies were picked into 96-well plates containing 300 µL of BG-11 with 6.35 ug ml^{-1} kanamycin or 3.125 ug ml^{-1} chloramphenicol. Concentrations of both respective antibiotics were gradually increased to 12.5 µg ml^{-1}. Cultures were verified for complete insertion via PCR and removed from antibiotics for experiments.

Growth Conditions. Both wild-type and mutant *Synechococcus elongatus* PCC7942 strains were grown in 125 mL culture flasks (Corning) in 50 mL BG-11 (Sigma) medium buffered with 1 g L^{-1} HEPES to pH 8.3 shaken at 130 rpm or on BG-11 plates containing 1.5% (w/v) agar. All strains were maintained and grown under constant LED illumination of 100 µE m^{-2} s^{-1} at either 20°C, 30°C, or 40°C in 2% or 0.04% CO_2 as specified. Cultures grown in 0.04% CO_2 were grown in air with no additional CO_2. Cultures were regularly diluted with fresh medium to maintain exponential growth phase for subsequent imaging and immunoblot analyses. For cloning, One Shot™ TOP10 Chemically Competent *E. coli* (ThermoFisher) were grown aerobically at 37° in Luria-Broth medium.

Fluorescence microscopy. Microscopy was performed using exponentially growing cells at an OD of 0.4. Two milliliters of culture were spun down at 15,000 x g for 60 s, resuspended in 100 µL of BG-11. Five microliters were transferred to a square 1.5% agarose + BG-11 pad, which was then flipped onto a 35 mm cell culture dish with a #1.5 glass coverslip bottom (ManTek). All images were captured using a Nikon Eclipse Ti2 inverted microscope with a PlanApo Objective lens (100x, 1.45NA, oil immersion), with phase contrast transillumination, and with a SOLA LED light source for imaging chlorophyll fluorescence (Excitation: 560/40nm (540-580nm), Emission: 630/70nm (593-668nm), Dichroic Mirror: 585nm) and RbcS-mTQ fluorescence (Excitation: 436/20nm (426-446nm), Emission: 480/40nm (460-500nm), Dichroic Mirror: 455nm). Images were acquired using a Photometrics Prime 95B Back-illuminated sCMOS Camera. Image analysis was performed using Fiji (Schindelin et al., 2012) and the MicrobeJ plugin (Ducret et al., 2016).

Growth Curve Measurements. Cultures were inoculated at a starting OD_{750} of 0.1-0.2 with fresh BG-11. Cell growth was monitored at OD_{750} using a DS-11 Spectrophotometer (DENOVI) at the specified time points. Growth rates were calculated using the linear portion of the

exponential phase of growth. Error bars represent the standard deviation from three biological replicates that were recorded from different culture flasks.

MicrobeJ quantification. Multiple fields of view were taken for each cell strain using three channels: Phase contrast provided cell perimeters, and fluorescence microscopy provided chlorophyll autofluorescence and RbcS-mTQ intensities. These data were analyzed using MicrobeJ (Ducret et al., 2016). In each cell-line, cell length detection was performed using the rod-shaped descriptor and thresholding set to 0.4µm < area < max, 0.71µm < width range < 2 µm, 0 µm < width variation < 0.2 µm, and 0 µm < angularity amplitude < 0.35 µm. Carboxysome detection was performed using the point function with a tolerance of 20 and an intensity minimum of 500. Associations, shape descriptors, profiles, and distances were recorded for each strain. All MicrobeJ quantification was also verified manually. Graphs were generated with Graph Pad Prism.

Immunoblot Analysis. Cells were lysed with a Qsonica sonication system (20 cycles - 30 s on, 10s off at 30% power) in 0.5 mL RuBisCO extraction buffer (50 mM EPPS at pH 8.1, 1% PVPP, 1 mM EDTA, 10 mM DTT, 0.1% Triton, and sigma protease inhibitor). Laemmli sample buffer (0.1 mL of 4x) was added to lysate prior to loading 10 µL on a 4%–12% Bis-Tris NuPAGE gel (Invitrogen). Gels were transferred onto a Mini-size polyvinylidene difluoride membrane (Bio-Rad) using a Trans-Blot Turbo system (Bio-Rad). The membrane was immunoprobed using rabbit polyclonal antisera against RbcL and the beta subunit of ATP synthase, AtpB (Agrisera) and then goat anti-rabbit IgG secondary antibody (LI-COR). Membrane signals were visualized and quantified at 600 nm using LI-COR Image Studio. For each sample, there were three replicates from the same cell lysate. We normalized RbcL signal using AtpB; a method previously used in Zhang *et al*., 2012 and specifically with *S. elongatus* PCC7942 in Sun *et al*., 2016 (Zhang et al., 2012; Sun et al., 2016).

ACKNOWLEDGMENTS
We would like to thank Drs. Lyle Simmons, Vincent Denef, and Daniel Ducat for providing critical feedback in experimental direction and data interpretation. We would also like to thank Pusparanee Anne Hakim for experimental assistance and critical reading of the manuscript.

REFERENCES:

Alvarado A, Kjær A, Yang W, Mann P, Briegel A, Waldor MK, Ringgaard S (2017) Coupling chemosensory array formation and localization. Elife. doi: 10.7554/eLife.31058

Atmakuri K, Cascales E, Burton OT, Banta LM, Christie PJ (2007) Agrobacterium ParA/MinD-like VirC1 spatially coordinates early conjugative DNA transfer reactions. EMBO J **26**: 2540–2551

Badrinarayanan A, Le TBK, Laub MT (2015) Bacterial Chromosome Organization and Segregation. Annu Rev Cell Dev Biol **31**: 171–199

Baxter JC, Funnell BE (2014) Plasmid Partition Mechanisms. Microbiol Spectr. doi: 10.1128/microbiolspec.PLAS-0023-2014

Bos J, Zhang Q, Vyawahare S, Rogers E, Rosenberg SM, Austin RH (2015) Emergence of antibiotic resistance from multinucleated bacterial filaments. Proc Natl Acad Sci **112**: 178 LP – 183

Broddrick JT, Welkie DG, Jallet D, Golden SS, Peers G, Palsson BO (2019) Predicting the metabolic capabilities of Synechococcus elongatus PCC 7942 adapted to different light regimes. Metab Eng. doi: 10.1016/j.ymben.2018.11.001

Burns RA, MacDonald CD, McGinn PJ, Campbell DA (2005) Inorganic carbon repletion disrupts photosynthetic acclimation to low temperature in the cyanobacterium Synechococcus elongatus. J Phycol. doi: 10.1111/j.1529-8817.2005.04101.x

Cameron JC, Wilson SC, Bernstein SL, Kerfeld CA (2013) Biogenesis of a Bacterial Organelle: The Carboxysome Assembly Pathway. Cell **155**: 1131–1140

Cayron J, Dedieu A, Lesterlin C (2020) Bacterial filament division dynamics allows rapid post-stress cell proliferation. bioRxiv 2020.03.16.993345

Chen B, Liu H, Huang B, Wang J (2014) Temperature effects on the growth rate of marine picoplankton. Mar Ecol Prog Ser. doi: 10.3354/meps10773

Clerico EM, Ditty JL, Golden SS (2007) Specialized Techniques for Site-Directed Mutagenesis in Cyanobacteria. Humana Press, pp 155–171

Doney SC, Ruckelshaus M, Emmett Duffy J, Barry JP, Chan F, English CA, Galindo HM, Grebmeier JM, Hollowed AB, Knowlton N, et al (2012) Climate Change Impacts on Marine Ecosystems. Ann Rev Mar Sci. doi: 10.1146/annurev-marine-041911-111611

Ducret A, Quardokus EM, Brun Y V. (2016) MicrobeJ, a tool for high throughput bacterial cell detection and quantitative analysis. Nat Microbiol **1**: 1–7

Ensminger I, Busch F, Huner NPA (2006) Photostasis and cold acclimation: Sensing low temperature through photosynthesis. Physiol Plant. doi: 10.1111/j.1399-3054.2006.00627.x

Eppley R (1972) Temperature and phytoplankton growth in the sea. Fish. Bull.

Erb TJ, Zarzycki J (2018) A short history of RubisCO: the rise and fall (?) of Nature's predominant CO2 fixing enzyme. Curr Opin Biotechnol. doi: 10.1016/j.copbio.2017.07.017

Falkowski PG, Sukenik A, Herzig R (1989) Nitrogen limitation in Isochrysis Galbana (Haptophyceae). II. Relative abundance of chloroplast proteins. J Phycol. doi: 10.1111/j.1529-8817.1989.tb00252.x

Fernández-González C, Pérez-Lorenzo M, Pratt N, Moore CM, Bibby TS, Marañón E (2020) Effects of Temperature and Nutrient Supply on Resource Allocation, Photosynthetic Strategy, and Metabolic Rates of Synechococcus sp. J Phycol. doi: 10.1111/jpy.12983

Flombaum P, Gallegos JL, Gordillo RA, Rincón J, Zabala LL, Jiao N, Karl DM, Li WKW, Lomas MW, Veneziano D, et al (2013) Present and future global distributions of the

marine Cyanobacteria Prochlorococcus and Synechococcus. Proc Natl Acad Sci U S A. doi: 10.1073/pnas.1307701110

Flores E, Herrero A (2010) Compartmentalized function through cell differentiation in filamentous cyanobacteria. Nat Rev Microbiol **8**: 39–50

Freeman Rosenzweig ES, Xu B, Kuhn Cuellar L, Martinez-Sanchez A, Schaffer M, Strauss M, Cartwright HN, Ronceray P, Plitzko JM, Förster F, et al (2017) The Eukaryotic CO2-Concentrating Organelle Is Liquid-like and Exhibits Dynamic Reorganization. Cell **171**: 148-162.e19

Galmés J, Aranjuelo I, Medrano H, Flexas J (2013) Variation in Rubisco content and activity under variable climatic factors. Photosynth Res. doi: 10.1007/s11120-013-9861-y

Galmés J, Hermida-Carrera C, Laanisto L, Niinemets Ü (2016) A compendium of temperature responses of Rubisco kinetic traits: variability among and within photosynthetic groups and impacts on photosynthesis modeling. J Exp Bot **67**: 5067–5091

Geider RJ (1987) Light and Temperature Dependence of the Carbon to Chlorophyll a Ratio in Microalgae and Cyanobacteria: Implications for physiology and growth of phytoplankton. New Phytol. doi: 10.1111/j.1469-8137.1987.tb04788.x

Gibson DG, Young L, Chuang RY, Venter JC, Hutchison CA, Smith HO (2009) Enzymatic assembly of DNA molecules up to several hundred kilobases. Nat Methods. doi: 10.1038/nmeth.1318

Hahn MW, Moore ERB, Höfle MG (1999) Bacterial Filament Formation, a Defense Mechanism against Flagellate Grazing, Is Growth Rate Controlled in Bacteria of Different Phyla. Appl Environ Microbiol **65**: 25 LP – 35

Heinrich K, Leslie DJ, Morlock M, Bertilsson S, Jonas K (2019) Molecular basis and ecological relevance of Caulobacter cell filamentation in freshwater habitats. MBio. doi: 10.1128/mBio.01557-19

Hill NC, Tay JW, Altus S, Bortz DM, Cameron JC (2020) Life cycle of a cyanobacterial carboxysome. Sci Adv **6**: eaba1269

Horvath DJ, Li B, Casper T, Partida-Sanchez S, Hunstad DA, Hultgren SJ, Justice SS (2011) Morphological plasticity promotes resistance to phagocyte killing of uropathogenic Escherichia coli. Microbes Infect **13**: 426–437

Huang S, Wilhelm SW, Harvey HR, Taylor K, Jiao N, Chen F (2012) Novel lineages of prochlorococcus and synechococcus in the global oceans. ISME J. doi: 10.1038/ismej.2011.106

Itakura AK, Chan KX, Atkinson N, Pallesen L, Wang L, Reeves G, Patena W, Caspari O, Roth R, Goodenough U, et al (2019) A Rubisco-binding protein is required for normal pyrenoid number and starch sheath morphology in Chlamydomonas reinhardtii Proc Natl Acad Sci **116**: 18445 LP – 18454

Jordan A, Chandler J, MacCready JS, Huang J, Osteryoung KW, Ducat DC (2017) Engineering Cyanobacterial Cell Morphology for Enhanced Recovery and Processing of Biomass. Appl Env Microbiol. doi: 10.1128/aem.00053-17

Justice SS, Hung C, Theriot JA, Fletcher DA, Anderson GG, Footer MJ, Hultgren SJ (2004) Differentiation and developmental pathways of uropathogenic Escherichia coli in urinary tract pathogenesis. Proc Natl Acad Sci **101**: 1333–1338

Justice SS, Hunstad DA, Cegelski L, Hultgren SJ (2008) Morphological plasticity as a bacterial survival strategy. Nat Rev Microbiol **6**: 162–168

Kaplan-Levy RN, Hadas O, Summers ML, Rücker J, Sukenik A (2010) Akinetes: Dormant

Cells of Cyanobacteria BT - Dormancy and Resistance in Harsh Environments. *In* E Lubzens, J Cerda, M Clark, eds,Springer Berlin Heidelberg, Berlin, Heidelberg, pp 5–27

Kerfeld CA, Melnicki MR (2016) Assembly, function and evolution of cyanobacterial carboxysomes. Curr Opin Plant Biol **31**: 66–75

Kratsch HA, Wise RR (2000) The ultrastructure of chilling stress. Plant Cell Environ **23**: 337–350

Kreuzer KN (2013) DNA Damage Responses in Prokaryotes: Regulating Gene Expression, Modulating Growth Patterns, and Manipulating Replication Forks. Cold Spring Harb Perspect Biol . doi: 10.1101/cshperspect.a012674

Kusumoto A, Shinohara A, Terashima H, Kojima S, Yakushi T, Homma M (2008) Collaboration of FlhF and FlhG to regulate polarflagella number and localization in Vibrio alginolyticus. Microbiology. doi: 10.1099/mic.0.2007/012641-0

Kysela DT, Randich AM, Caccamo PD, Brun Y V (2016) Diversity Takes Shape: Understanding the Mechanistic and Adaptive Basis of Bacterial Morphology. PLOS Biol **14**: e1002565

Lee KP, Kim C, Landgraf F, Apel K (2007) EXECUTER1- and EXECUTER2-dependent transfer of stress-related signals from the plastid to the nucleus of Arabidopsis thaliana Proc Natl Acad Sci **104**: 10270 LP – 10275

Liao Y, Rust MJ (2018) The Min Oscillator Defines Sites of Asymmetric Cell Division in Cyanobacteria during Stress Recovery. Cell Syst. doi: 10.1016/j.cels.2018.10.006

Losh JL, Morel FMM, Hopkinson BM (2012) Modest increase in the C:N ratio of N-limited phytoplankton in the California Current in response to high CO2. Mar Ecol Prog Ser. doi: 10.3354/meps09981

Losh JL, Young JN, Morel FMM (2013) Rubisco is a small fraction of total protein in marine phytoplankton. New Phytol. doi: 10.1111/nph.12143

MacCready JS, Basalla JL, Vecchiarelli AG (2020) Origin and Evolution of Carboxysome Positioning Systems in Cyanobacteria. Mol Biol Evol **37**: 1434–1451

MacCready JS, Hakim P, Young EJ, Hu L, Liu J, Osteryoung KW, Vecchiarelli AG, Ducat DC (2018) Protein gradients on the nucleoid position the carbon-fixing organelles of cyanobacteria. Elife. doi: 10.7554/eLife.39723

MacCready JS, Vecchiarelli AG (2018) In long bacterial cells, the Min system can act off-center. Mol Microbiol **109**: 268–272

Muraleedharan S, Freitas C, Mann P, Glatter T, Ringgaard S (2018) A cell length-dependent transition in MinD-dynamics promotes a switch in division-site placement and preservation of proliferating elongated Vibrio parahaemolyticus swarmer cells. Mol Microbiol **109**: 365–384

Murayama Y, Kori H, Oshima C, Kondo T, Iwasaki H, Ito H (2017) Low temperature nullifies the circadian clock in cyanobacteria through Hopf bifurcation. Proc Natl Acad Sci U S A. doi: 10.1073/pnas.1620378114

Ohbayashi R, Nakamachi A, Hatakeyama TS, Watanabe S, Kanesaki Y, Chibazakura T, Yoshikawa H, Miyagishima S (2019) Coordination of Polyploid Chromosome Replication with Cell Size and Growth in a Cyanobacterium. MBio. doi: 10.1128/mbio.00510-19

Oltrogge LM, Chaijarasphong T, Chen AW, Bolin ER, Marqusee S, Savage DF (2020) Multivalent interactions between CsoS2 and Rubisco mediate α-carboxysome formation. Nat Struct Mol Biol **27**: 281–287

Perez-Cheeks BA, Planet PJ, Sarkar IN, Clock SA, Xu Q, Figurski DH (2012) The product

of tadZ, a new member of the parA/minD superfamily, localizes to a pole in Aggregatibacter actinomycetemcomitans. Mol Microbiol **83**: 694–711

Pernthaler J (2005) Predation on prokaryotes in the water column and its ecological implications. Nat Rev Microbiol **3**: 537–546

Pernthaler J, Zöllner E, Warnecke F, Jürgens K (2004) Bloom of filamentous bacteria in a mesotrophic lake: Identity and potential controlling mechanism. Appl Environ Microbiol **70**: 6272–6281

Rae BD, Long BM, Badger MR, Price GD (2013) Functions, compositions, and evolution of the two types of carboxysomes: Polyhedral microcompartments that facilitate CO2 fixation in cyanobacteria and some proteobacteria. Microbiol Mol Biol Rev. doi: 10.1128/MMBR.00061-12

Raghunathan S, Chimthanawala A, Krishna S, Vecchiarelli AG, Badrinarayanan A (2020) Asymmetric chromosome segregation and cell division in DNA damage-induced bacterial filaments. bioRxiv 2020.03.16.993485

Raskin DM, De Boer PAJ (1999) Rapid pole-to-pole oscillation of a protein required for directing division to the middle of Escherichia coli. Proc Natl Acad Sci U S A. doi: 10.1073/pnas.96.9.4971

Raven JA, Geider RJ (1988) Temperature and algal growth. New Phytol. doi: 10.1111/j.1469-8137.1988.tb00282.x

Raven JA, Johnston AM (1991) Mechanisms of inorganic-carbon acquisition in marine phytoplankton and their implications for the use of other resources. Limnol Oceanogr. doi: 10.4319/lo.1991.36.8.1701

Ringgaard S, Schirner K, Davis BM, Waldor MK (2011) A family of ParA-like ATPases promotes cell pole maturation by facilitating polar localization of chemotaxis proteins. Genes Dev **25**: 1544–1555

Savage DF, Afonso B, Chen AH, Silver PA (2010) Spatially Ordered Dynamics of the Bacterial Carbon Fixation Machinery. Science (80-) **327**: 1258–1261

Schindelin J, Arganda-Carreras I, Frise E, Kaynig V, Longair M, Pietzsch T, Preibisch S, Rueden C, Saalfeld S, Schmid B, et al (2012) Fiji: an open-source platform for biological-image analysis. Nat Methods **9**: 676–682

Shih PM, Wu D, Latifi A, Axen SD, Fewer DP, Talla E, Calteau A, Cai F, Tandeau De Marsac N, Rippka R, et al (2013) Improving the coverage of the cyanobacterial phylum using diversity-driven genome sequencing. Proc Natl Acad Sci U S A. doi: 10.1073/pnas.1217107110

Simek K, Vrba J, Pernthaler J, Posch T, Hartman P, Nedoma J, Psenner R (1997) Morphological and compositional shifts in an experimental bacterial community influenced by protists with contrasting feeding modes. Appl Environ Microbiol **63**: 587 LP – 595

Singh SP, Montgomery BL (2011) Determining cell shape: adaptive regulation of cyanobacterial cellular differentiation and morphology. Trends Microbiol **19**: 278–285

Sun Y, Casella S, Fang Y, Huang F, Faulkner M, Barrett S, Liu LN (2016) Light modulates the biosynthesis and organization of cyanobacterial carbon fixation machinery through photosynthetic electron flow. Plant Physiol **171**: 530–541

Sun Y, M Wollman AJ, Huang F, Leake MC, Liu L-N (2019) Single-Organelle Quantification Reveals Stoichiometric and Structural Variability of Carboxysomes Dependent on the Environment. Plant Cell Adv Publ. doi: 10.1105/tpc.18.00787

Tabita FR, Hanson TE, Satagopan S, Witte BH, Kreel NE (2008) Phylogenetic and

evolutionary relationships of RubisCO and the RubisCO-like proteins and the functional lessons provided by diverse molecular forms. Philos Trans R Soc B Biol Sci. doi: 10.1098/rstb.2008.0023

Thompson SR, Wadhams GH, Armitage JP (2006) The positioning of cytoplasmic protein clusters in bacteria. Proc Natl Acad Sci USA **103**: 8209–8214

Viollier PH, Sternheim N, Shapiro L (2002) Identification of a localization factor for the polar positioning of bacterial structural and regulatory proteins. Proc Natl Acad Sci USA **99**: 13831–13836

Wang H, Yan X, Aigner H, Bracher A, Nguyen ND, Hee WY, Long BM, Price GD, Hartl FU, Hayer-Hartl M (2019) Rubisco condensate formation by CcmM in beta-carboxysome biogenesis. Nature **566**: 131–135

Wehrens M, Ershov D, Rozendaal R, Walker N, Schultz D, Kishony R, Levin PA, Tans SJ (2018) Size Laws and Division Ring Dynamics in Filamentous Escherichia coli cells. Curr Biol **28**: 972-979.e5

Welkie DG, Rubin BE, Diamond S, Hood RD, Savage DF, Golden SS (2019) A Hard Day's Night: Cyanobacteria in Diel Cycles. Trends Microbiol. doi: 10.1016/j.tim.2018.11.002

Wortinger MA, Quardokus EM, Brun Y V (1998) Morphological adaptation and inhibition of cell division during stationary phase in Caulobacter crescentus. Mol Microbiol **29**: 963–973

Yang DC, Blair KM, Salama NR (2016) Staying in Shape: the Impact of Cell Shape on Bacterial Survival in Diverse Environments. Microbiol Mol Biol Rev **80**: 187 LP – 203

Youderian P, Burke N, White DJ, Hartzell PL (2003) Identification of genes required for adventurous gliding motility in Myxococcus xanthus with the transposable element mariner. Mol Microbiol **49**: 555

Young JN, Goldman JAL, Kranz SA, Tortell PD, Morel FMM (2015) Slow carboxylation of Rubisco constrains the rate of carbon fixation during Antarctic phytoplankton blooms. New Phytol. doi: 10.1111/nph.13021

Yu J, Liberton M, Cliften PF, Head RD, Jacobs JM, Smith RD, Koppenaal DW, Brand JJ, Pakrasi HB (2015) Synechococcus elongatus UTEX 2973, a fast growing cyanobacterial chassis for biosynthesis using light and CO_2. Sci Rep. doi: 10.1038/srep08132

Zhang P, Eisenhut M, Brandt AM, Carmel D, Silén HM, Vass I, Allahverdiyeva Y, Salminen TA, Aro EM (2012) Operon flv4-flv2 provides cyanobacterial photosystem ii with flexibility of electron transfer. Plant Cell. doi: 10.1105/tpc.111.094417

Table 1: Strains used in this study

Strain	**Description**	**Source**
Synechococcus elongatus PCC7942	Wild Type	-
Synechococcus elongatus PCC7942	Δ*mcdA*	(MacCready et al., 2018)
Synechococcus elongatus PCC7942	Δ*mcdB*	(MacCready et al., 2018)
Synechococcus elongatus PCC7942	Δ*mcdAB*	(MacCready et al., 2018)
Synechococcus elongatus PCC7942	*rbcS-mTQ*	Wild Type transformed with pAH40
Synechococcus elongatus PCC7942	Δ*mcdA* + *rbcS-mTQ*	Δ*mcdA* transformed with pAH40
Synechococcus elongatus PCC7942	Δ*mcdB* + *rbcS-mTQ*	Δ*mcdB* transformed with pAH40
Synechococcus elongatus PCC7942	Δ*mcdAB* + *rbcS-mTQ*	Δ*mcdA*B transformed with pAH40

FIGURES AND FIGURE LEGENDS

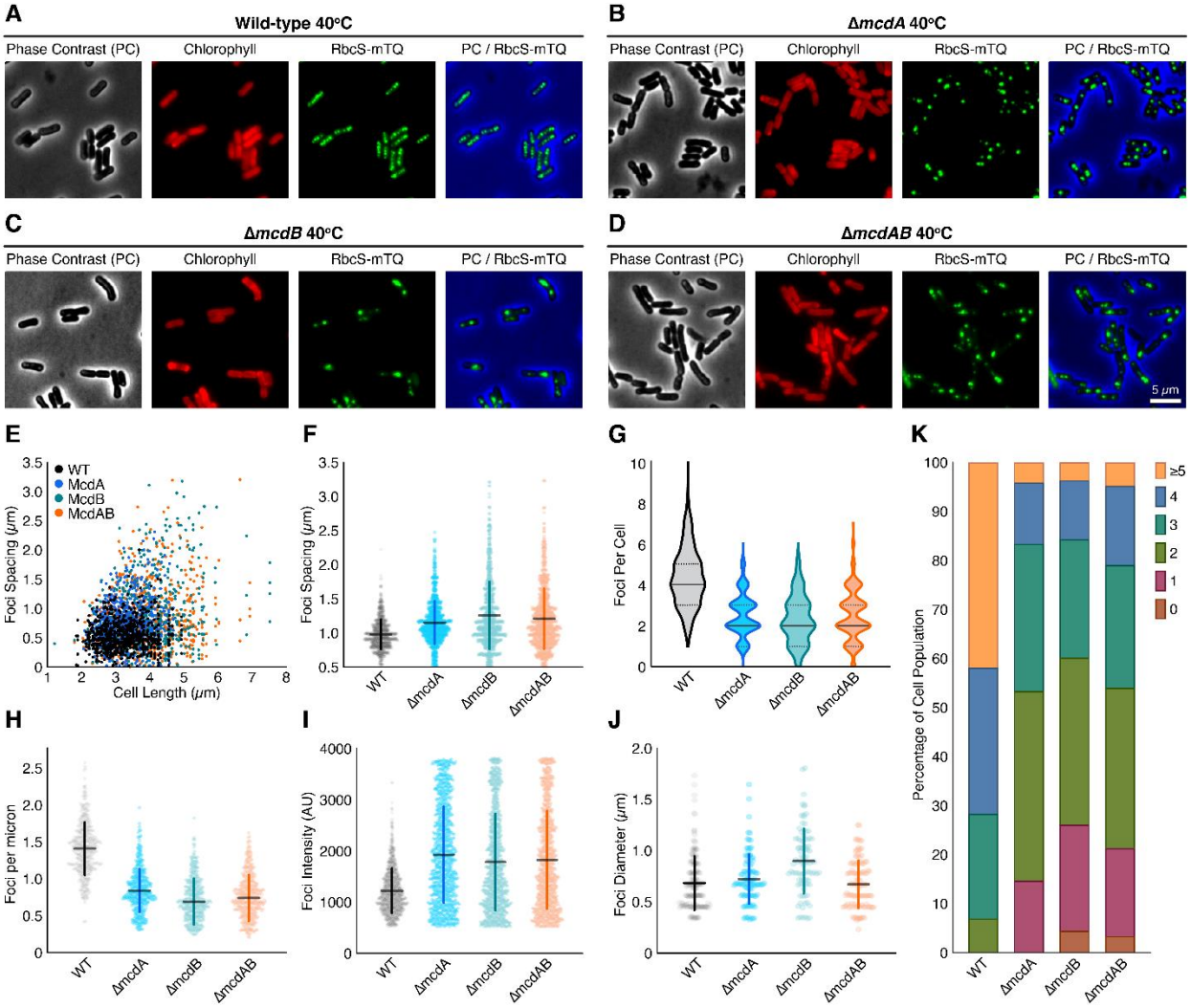

Figure 1. At 40°C Mcd system mutants display fewer, asymmetrically-positioned carboxysome aggregates. (**A-D**) Microscopy images of the specified cell strains. Phase contrast (black), chlorophyll (red), and carboxysomes (green). Phase Contrast (PC) channel is blue in the merge. (**E**) Quantification of spacing between carboxysome foci as a function of the cell length. (**F**) Violin plot of spacing between carboxysome foci. (**G**) Violin plot of carboxysome foci number per cell. (**H**) Violin plot of number of carboxysome foci in a cell as a function of cell length. (**I**) Carboxysome peak foci intensity for each cell strain. Arbitrary Units (AU). (**J**) Quantification of carboxysome foci diameter ($n \geq 93$). (**K**) Population percentages of cells with the specified number of carboxysome foci. (**A-K**) Cells were grown at 40°C in 2% CO_2. $n \geq 1000$ carboxysomes from 440 cells. Error bars = Standard deviation.

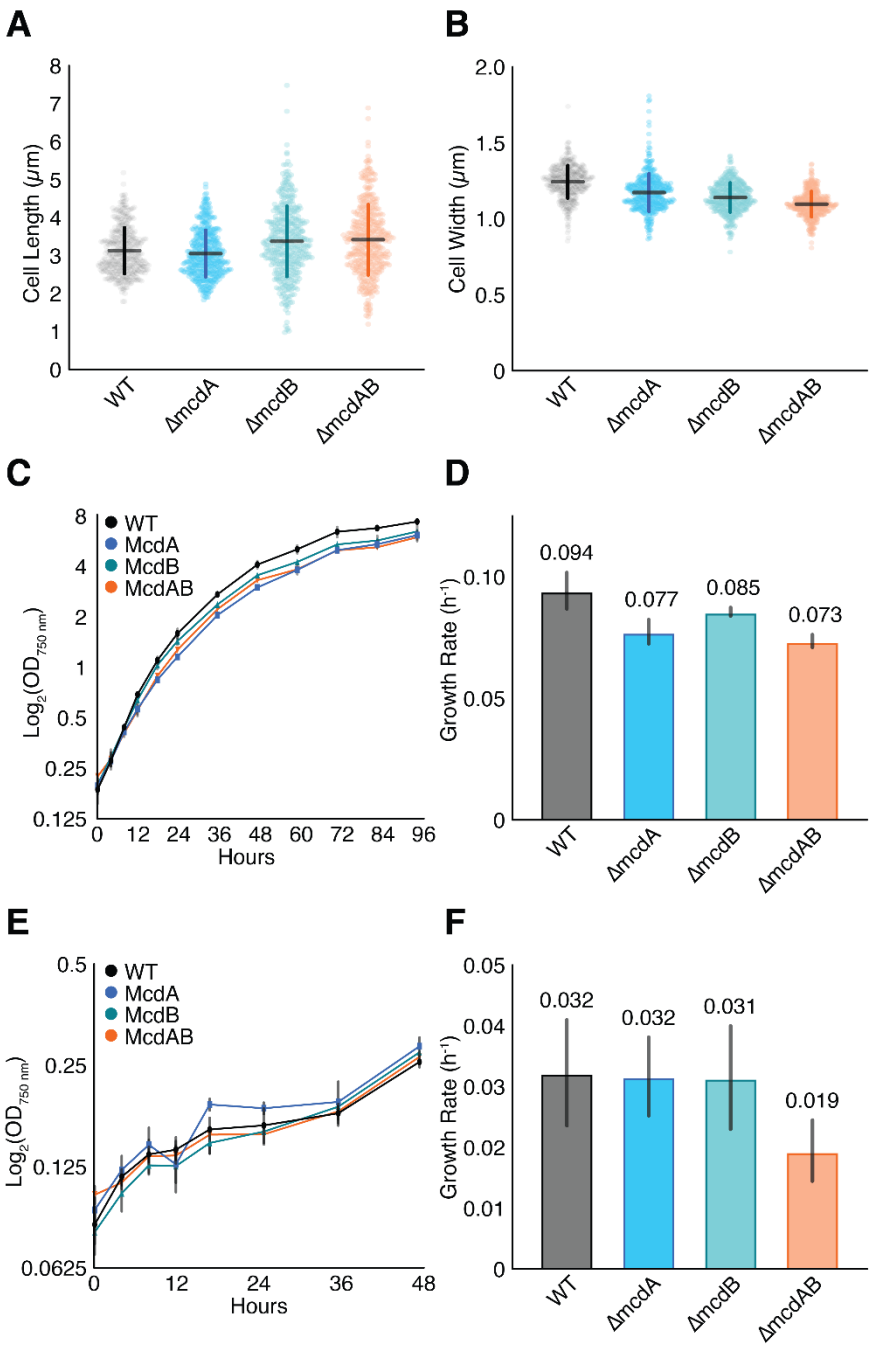

Figure 2. At 40°C carboxysome mispositioning correlate with subtle changes in cell morphology. (**A**) Violin plot of cell length. (**B**) Violin plot of cell width. (**A** and **B**) Cells were grown at 40°C in 2% CO_2. n = 440 cells. (**C**) Growth curve of all strains grown at 40°C in 2% CO_2. (**D**) Quantification of exponential growth rate at 40°C in 2% CO_2. (**E**) Growth curve of all strains grown at 40°C in 0.4% CO_2. (**F**) Quantification of exponential growth rate at 40°C in 0.4% CO_2. Error bars represent the standard deviation from three independent biological replicates.

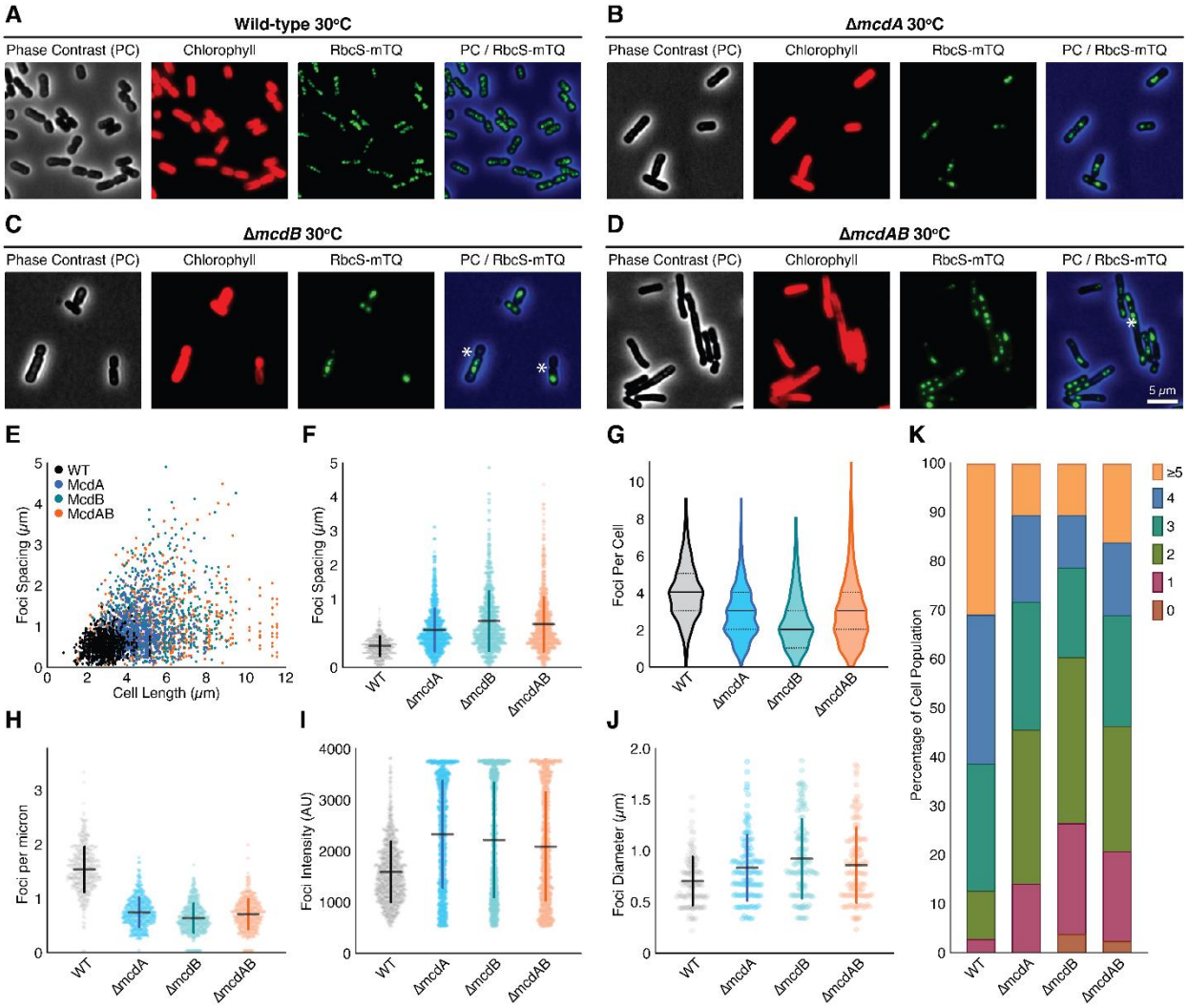

Figure 3. At 30°C Mcd system mutants display fewer, asymmetrically-positioned carboxysome aggregates. (**A-D**) Microscopy images of the specified cell strains. Phase contrast (black), chlorophyll (red), and carboxysomes (green). Phase Contrast (PC) channel is blue in the merge. Asterisks highlight asymmetric cell division events. (**E**) Quantification of spacing between carboxysome foci as a function of the cell length. (**F**) Violin plot of spacing between carboxysome foci. (**G**) Violin plot of carboxysome foci per cell. (**H**) Violin plot of number of carboxysome foci in a cell as a function of cell length. (**I**) Carboxysome peak foci intensity. Arbitrary Units (AU). (**J**) Quantification of carboxysome foci diameter ($n \geq 100$). (**K**) Population percentages of cells with the specified number of carboxysome foci. (**A-K**) Cells were grown at 30°C in 2% CO_2. $n \geq 1200$ carboxysomes from 486 cells. Error bars = Standard deviation.

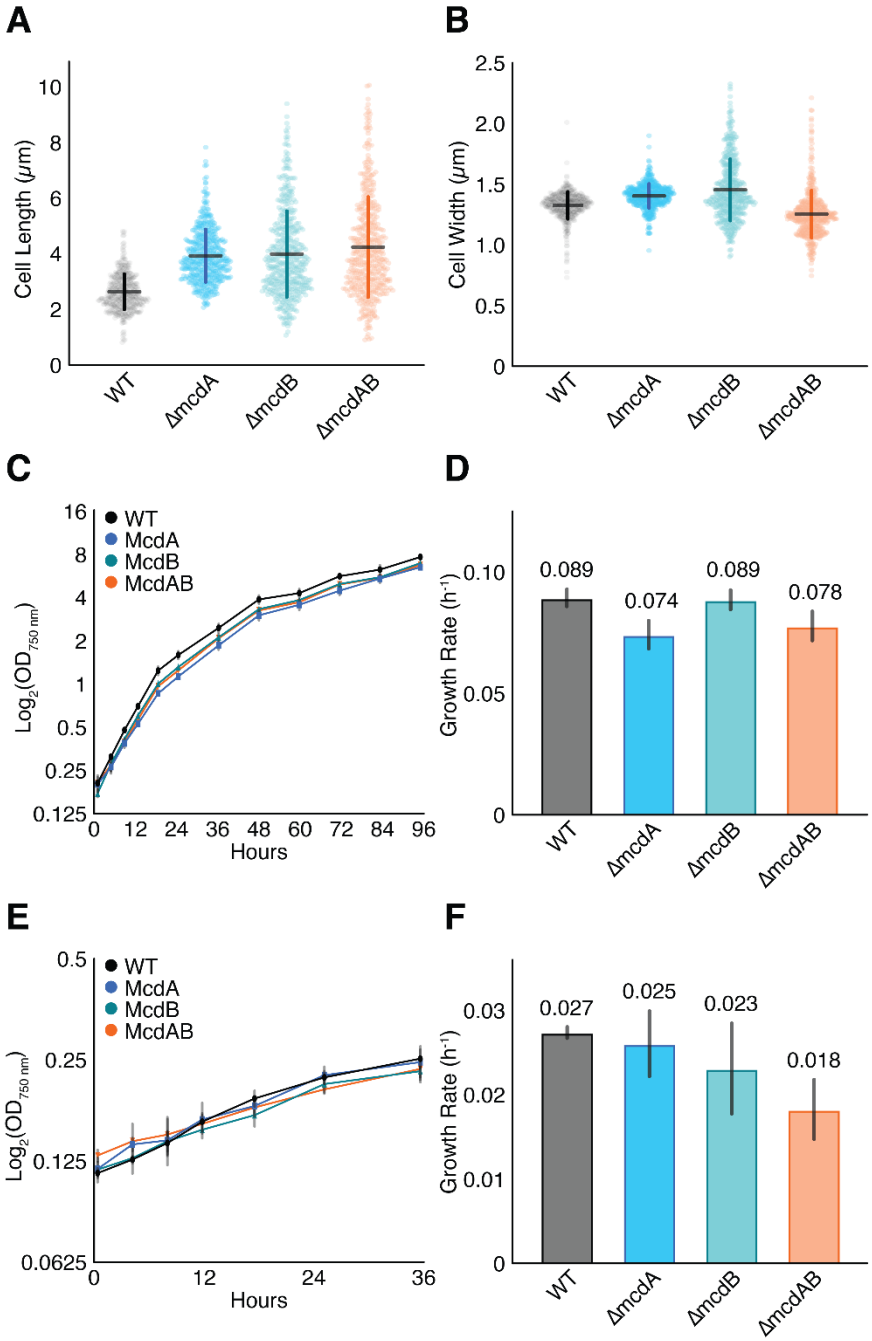

Figure 4. At 30°C Mcd mutants grow slower and are elongated. (**A**) Violin plot of cell length. (**B**) Violin plot of cell width. (**A** and **B**) Cells were grown at 30°C in 2% CO_2. n = 486 cells. (**C**) Growth curve of all strains grown at 30°C in 2% CO_2. (**D**) Quantification of exponential growth rate at 30°C in 2% CO_2. (**E**) Growth curve of all strains grown at 30°C in 0.4% CO_2. (**F**) Quantification of exponential growth rate at 30°C in 0.4% CO_2. (**C-F**) Error bars represent the standard deviation from three independent biological replicates.

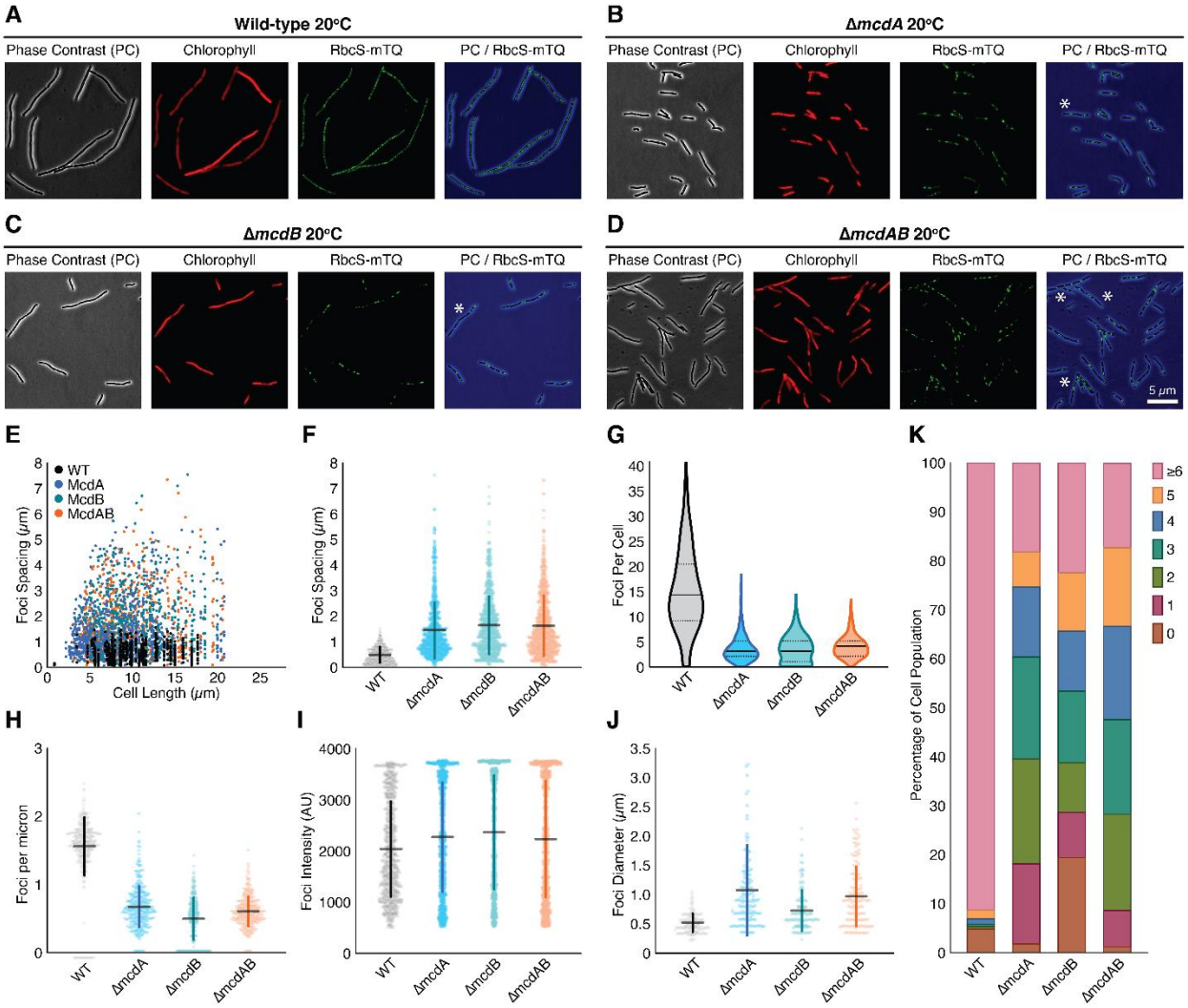

Figure 5. At 20°C wild-type and Mcd system mutants elongate, but only the mutants display fewer, asymmetrically-positioned carboxysome aggregates. (**A-D**) Microscopy images of the specified cell strains. Phase contrast (black), chlorophyll (red), and carboxysomes (green). Phase Contrast (PC) channel is blue in the merge. Asterisks highlight asymmetric division events. (**E**) Quantification of spacing between carboxysome foci as a function of the cell length. (**F**) Violin plot of spacing between carboxysome foci. (**G**) Violin plot of carboxysome foci per cell. (**H**) Violin plot of number of carboxysome foci in a cell as a function of cell length. (**I**) Carboxysome peak foci intensity. Arbitrary Units (AU). (**J**) Quantification of carboxysome foci diameter ($n \geq 100$). (**K**) Population percentages of cells with specified number of carboxysome foci. Cells were grown at 20°C in 2% CO_2. $n \geq 1000$ carboxysomes from n = 338 cells. Error bars = Standard deviation.

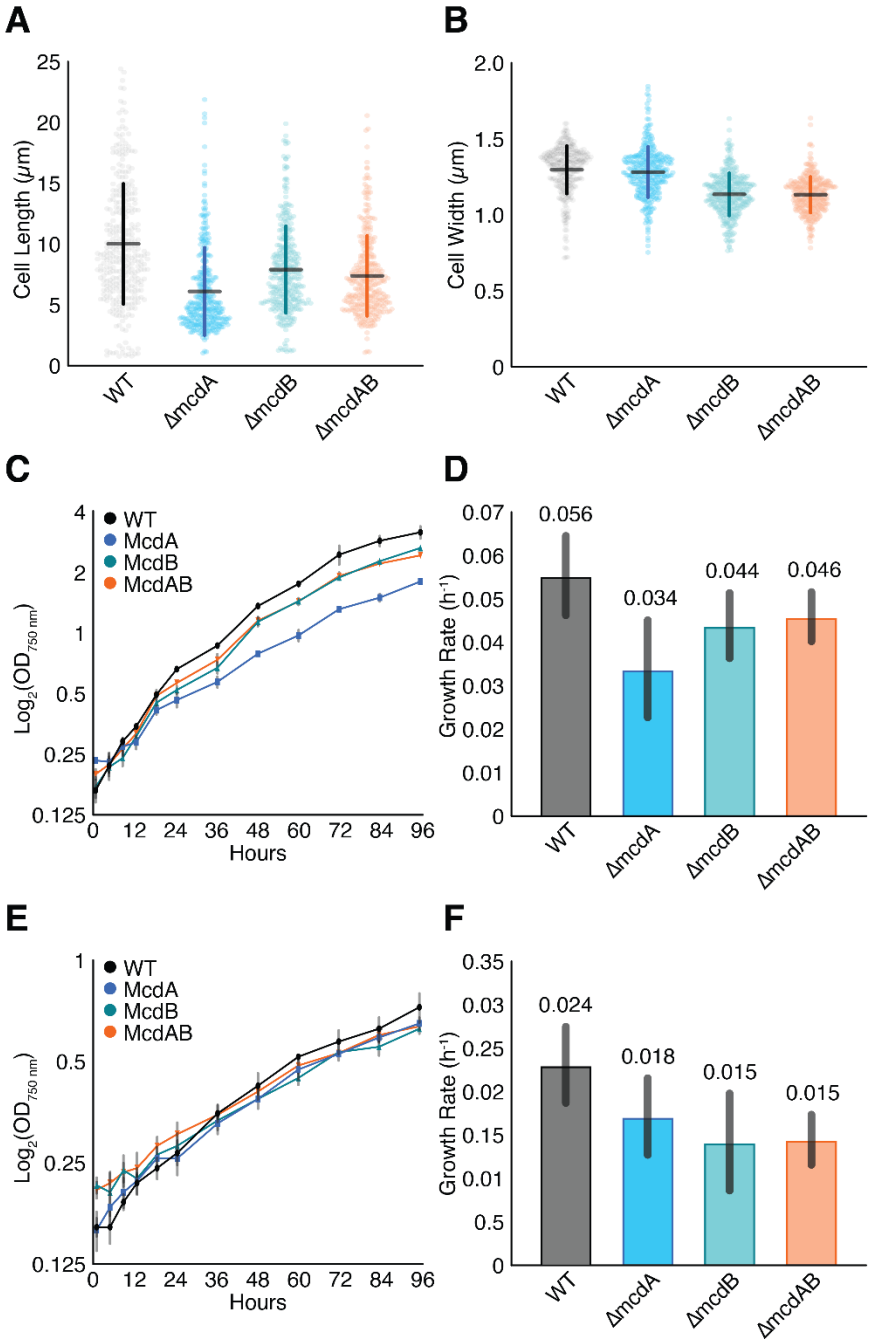

Figure 6. At 20°C wild-type and Mcd system mutants elongate, but the mutants display slower growth rates. (**A**) Violin plot of cell length for cell strains. (**B**) Violin plot of cell width for cells strains. (**A** and **B**) Cells were grown at 20°C in 2% CO_2. n = 338 cells. (**C**) Growth curve of all strains grown at 30°C in 2% CO_2. (**D**) Quantification of exponential growth rate at 20°C in 2% CO_2. (**E**) Growth curve of all strains grown at 30°C in 0.4% CO_2. (**F**) Quantification of exponential growth rate at 20°C in 0.4% CO_2. (**C-F**) Error bars represent the standard deviation from three independent biological replicates.

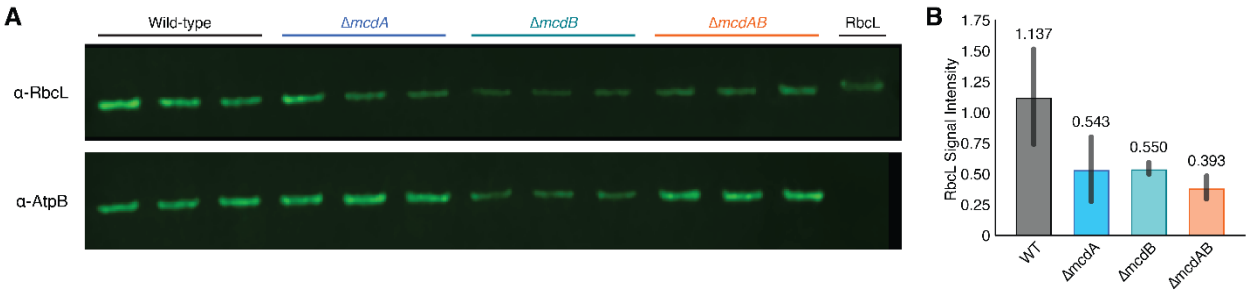

Figure 7. Mcd mutants have decreased cellular levels of RuBisCO. (**A**) Western Blot analysis of RbcL signal (top) and Atpß (bottom). Wild-type (lanes 1-3), Δ*mcdA* (lanes 4-6), Δ*mcdB* (lanes 7-9), and Δ*mcdAB* (lanes 10-12), purified RbcL control (lane 13). (**B**) Quantification of immunoblot signal for each cell type specified. Cells were grown at 30°C in 2% CO_2.

Supplemental Figure

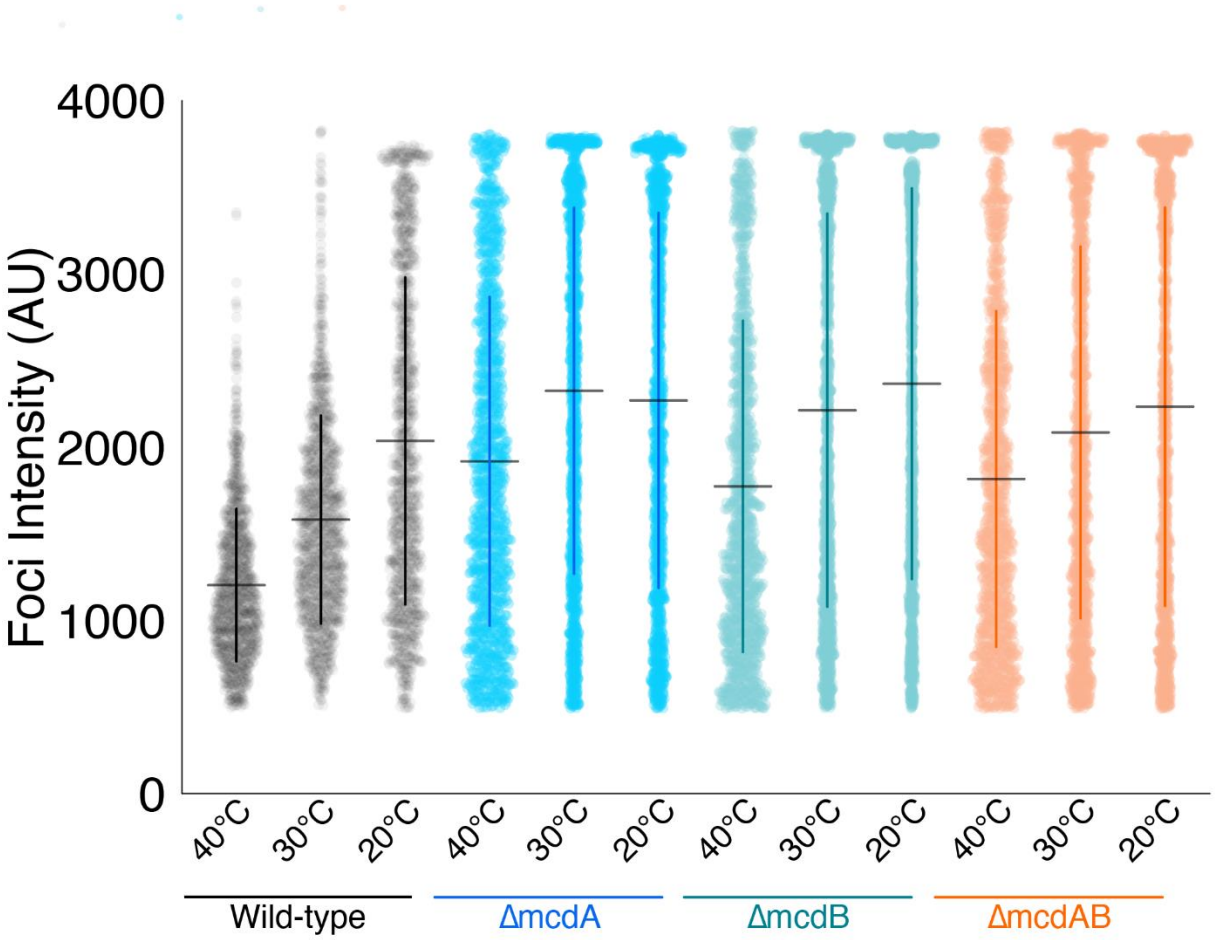

Figure S1. Comparison of the peak RbcS-mTQ focus intensities. Arbitrary Units (AU). n > 1000 carboxysomes per cell-line at each temperature.